J. Fluid Mech. (1974), *vol.* 65, *part* 3, *pp.* 541–560
Printed in Great Britain

Unstable waves on an axisymmetric jet column

By G. E. MATTINGLY AND C. C. CHANG
Department of Civil and Geological Engineering, Princeton University

(Received 14 May 1973 and in revised form 13 November 1973)

The growth of infinitesimal disturbances on an axisymmetric jet column is investigated theoretically and experimentally. The theoretical analysis is based upon inviscid stability theory, wherein axisymmetric, helical and double helical disturbances are considered from the spatial reference frame. In the jet flow field near the source, the mean velocity profile is observed to have a potential core and a thin, but finite, shear layer between the potential core and the quiescent ambient fluid. With downstream distance, the potential core diameter decreases and the shear-layer thickness increases. To incorporate these variations into the theory, a quasi-uniform assumption is adopted, whereby successive velocity profiles are analysed individually throughout the region in the jet flow where disturbances are observed to be small. The results of the theory indicate that initially, in the jet flow where the shear layer is thin and the potential core is larger, all disturbances considered are unstable. The dominant disturbance in the jet is an axisymmetric one. However, further downstream in the jet, where the half-breadth thickness of the shear layer is 55 % of the potential core radius, a helical disturbance is found to dominate the axisymmetric and double helical modes. Nowhere in the jet flow field examined was the double helical disturbance found to be dominant. The cross-stream distributions of velocity and vorticity for the dominant disturbance modes are presented according to the spatial stability theory.

The downstream development of the jet column and the characteristics of the disturbances amplifying on it were also studied in a water tank. No artificial stimulation of any particular disturbance was used. The experimental results show good agreement with the results of the theory in the region where the disturbances are small. However, conclusive confirmation of the switch in the hierarchy of dominant disturbances was not found. Half of the time the disturbance observed experimentally exhibits an axisymmetric character and the other half a helical one. This apparently is due to the similar spatial amplification rates experienced by both of these disturbance modes. It is concluded that this switching of dominant modes is, in large part, responsible for (i) the well-known natural drifting of disturbance characteristics in jet flows, and (ii) the wide variety of observations made in previous jet experiments.

1. Introduction

It has been known for well over one hundred years that the laminar, axisymmetric jet is unstable at high Reynolds number, and that the shear layers are rolled up into vortices before turbulence is observed. Batchelor & Gill (1962) attempted to predict theoretically, via linearized stability theory, the disturbance characteristics observed in the axisymmetric jet experiment conducted by Reynolds (1962). Their analysis considered the stability of three different types of disturbances in the jet flow. The first was an axisymmetric (or varicose) disturbance, the second a helical and the third a double helical disturbance. Their results pertained to (i) the so-called 'top-hat' jet comprised of a potential core inside an infinitesimally thin shear layer, and (ii) a 'far-downstream' profile which has no potential core and a shear layer of finite thickness. For the 'top-hat' jet, they found that all three types of disturbances satisfy their necessary condition for instability. For the far-downstream profile, only sinuous or helical modes were found to be amplified. The particularly disturbing feature of the Batchelor & Gill theory was that it did not conclusively predict the experimental observations, namely the 'puffs' and 'condensations' (or axisymmetric disturbances) observed in a jet. Later, Gill (1962) incorporated viscous effects in an attempt to predict theoretically that axisymmetric disturbances are the most highly amplified in the jet flow. However, this effort also proved unsuccessful, with the conclusion drawn that perhaps small but finite disturbances of the axisymmetric variety would have to be considered if the theory were to predict the experimental observations.

In the dye study conducted by Reynolds, a variety of observations of jet breakup were noted through his Reynolds number range of 10 to 300^+, with his particular background conditions. With increasing flow rate, the jet was observed to have (i) tiny puffs of dye near the nozzle producing the jet, (ii) axisymmetric condensations away from the nozzle, (iii) sinuous undulations of long wavelength farther from the nozzle and finally foot-shaped dye pockets and then confused breakup. It should be noted that Reynolds did not use artificial stimulation to excite any particular disturbance. The present results extend the attempts of Batchelor & Gill, and Gill to explain these observations using stability theory.

When stability analyses are performed from the temporal viewpoint, the disturbances considered are permitted to oscillate both with distance in the stream direction and in time, and are unstable in the sense that they grow in an exponential envelope in time. Spatial stability, on the other hand, entertains disturbances which also oscillate in time and space, but either dampen or amplify exponentially in space. This latter type of stability analysis conforms immediately with what is observed experimentally (see Freymuth 1966). Of course, a Galilean transformation exists which connects the results of these two types of analyses. Gaster (1968) showed that the group velocity is the appropriate velocity for this transformation when the amplification rates are small. However, in the cases of highly unstable free shear layers, the proper velocity is difficult to obtain as it requires excessive computer time (see Mattingly & Criminale 1972).

The latter concluded, in fact, that the stability analysis should be performed

solely from the spatial viewpoint, as a result of the improved agreement they achieved with experimental values in their naturally amplifying wake flow. The present results indicate that, when the mean profile is properly described with a potential core and a thin but finite shear-layer region separating the core from the stationary, ambient fluid, agreement between the spatial theory and experimental observations is to be considered very good. In view of this, it is again concluded that stability analyses should be performed solely from the spatial viewpoint.

The present results contradict those of Crow & Champagne (1971), who concluded, from the disagreement between their phase velocity measurements and the predictions from their spatial theory applied to the 'top-hat' jet, that these analyses are to be done temporally. In addition, they bolstered this conclusion by suggesting that the spatial stability theory is mathematically inconsistent with downstream boundary conditions. The present authors feel that the choice of the 'top-hat' jet profile is both an unnecessary simplification of the actual distribution, and the cause of the phase velocity disagreement found by Crow & Champagne. Furthermore, they interpret the downstream boundary conditions in the spatial stability problem as the limit of linearity, thereby avoiding any mathematical inconsistency.

The present study includes a presentation of the cross-stream, as well as downstream, distributions of the disturbance velocity and vorticity. The authors feel that, with a thorough understanding of the dynamics of small disturbances in unstable fluid flows, there can be a continuous progression to the nonlinear analyses conducted downstream or to the initial conditions for numerical computations of such complex flows.

2. Experiment

2.1. *Description of facility*

The experiment was conducted in the John E. Nicholson Tilting Flume Facility of the Lewis F. Moody Hydrodynamics Laboratory at Princeton University. Mattingly (1968) describes this facility. A partition was installed across the (16 in. deep by 30 in. wide) flow section, and, with a suitable fairing surface, the 1 in. diameter, axisymmetric jet flow field was produced in the water at the centre of this partition. Visual observations of the flow field were made using the hydrogen-bubble flow visualization technique (see Mattingly 1966); detailed surveys were made using DISA dual-channel anemometry. Sensors used were DISA quartz-coated fibres; these were traversed with accuracies of 0·001 and 0·002 in. in the radial and longitudinal directions, respectively. The jet flow field, as seen using the hydrogen-bubble technique, is shown in figure 1 (plate 1). To achieve low values of turbulence intensity at the nozzle exit, the centre-line velocity was less than $0{\cdot}5\,\mathrm{in.s^{-1}}$, giving a diametral Reynolds number of 300, which is considered sufficiently large to correspond to the inviscid theory.

2.2. *Survey of the jet flow field*

The general aspects of the amplitudes and frequencies of the longitudinal disturbance velocity $\tilde{V}_Z$ are shown in the fluctuation map, figure 2. Traced oscillographic

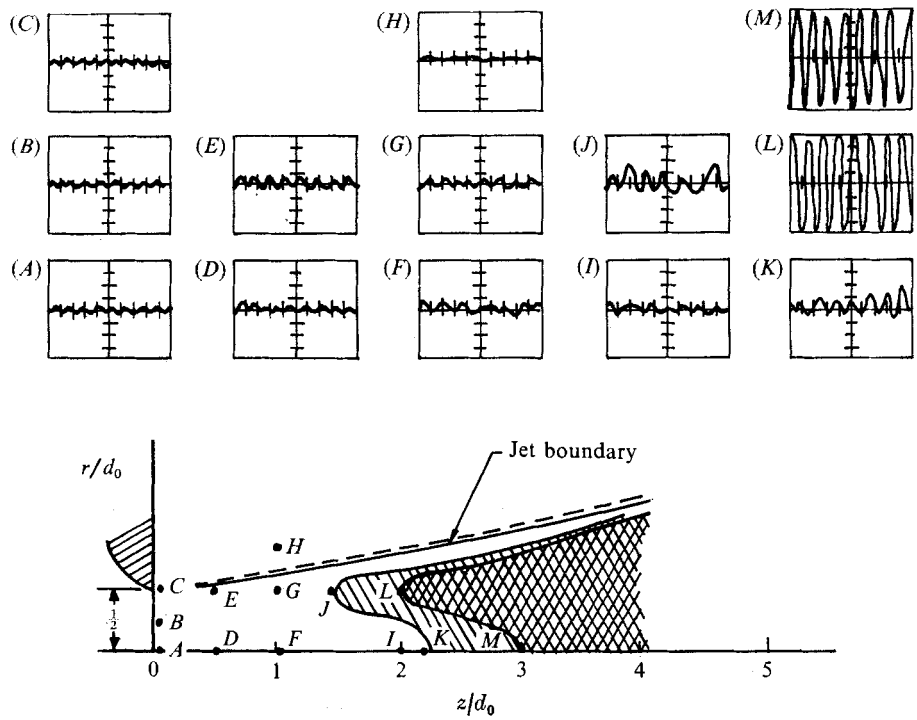

FIGURE 2. Fluctuation map. ▧, region where disturbed amplitudes equal or exceed 1 % of the centre-line velocity; ▨, region where disturbances equal or exceed 4 % of the centre-line velocity. Grid marks on each oscillograph denote: vertically 1 % of centre-line velocity, horizontally 0·1 s.

records of anemometer response are presented to indicate that, within the first two diameters of the jet flow field, the periodic disturbance level is less than 2·3 % of the jet's potential core velocity. It is assumed that this small amplitude justifies the use of the linearized stability theory in this region.

In the present investigation, considerable care was taken to avoid spurious vibrations in the jet profile. A turbulence level of 0·1 % existed at the nozzle exit, and no artifical excitation was used in any way to stabilize the natural jet frequency.

The results of the mean profile measurements are presented in figure 3. To facilitate computer calculation of the eigenvalues, these profiles were smoothed, so that both the potential core and the important shear layer at the edge of the jet were properly included. Consequently, two parameters are required for each profile: one for the radius of the potential core, the other to specify the shear-layer structure using a one-sided Gaussian distribution, i.e.

$$U(R) = 1{\cdot}0 \quad (0 \leqslant R \leqslant A), \qquad U(R) = \exp\{-\sigma(R-A)^2\} \quad (R \geqslant A). \quad (2.2.1)$$

The values for the potential core radius A are presented in table 1. The co-ordinates (R, Z) and radius A are non-dimensionalized, using the local half-breadth thickness of the jet's shear layer, a procedure which produced $\sigma = 0{\cdot}693$, a constant.

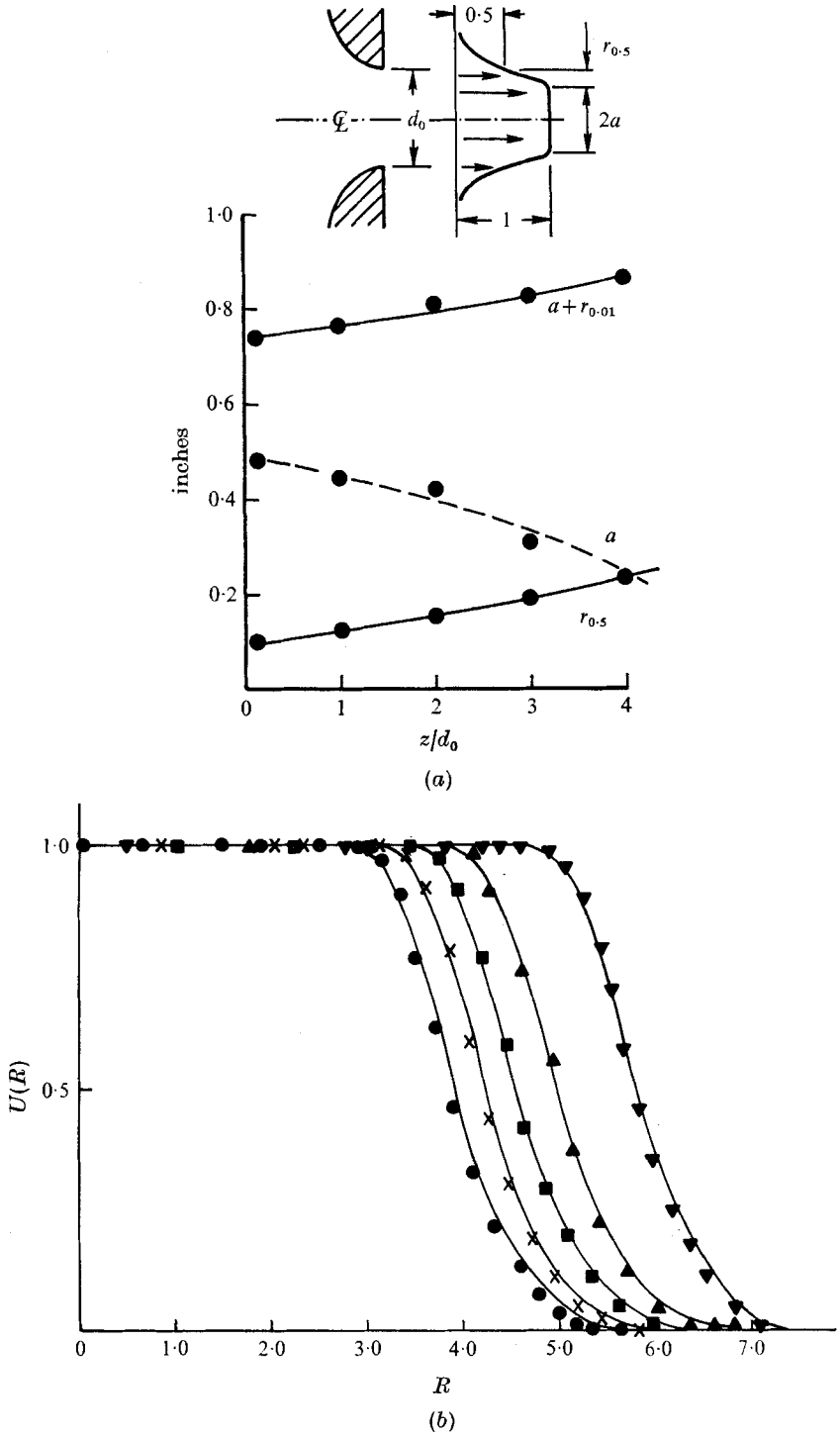

FIGURE 3. (*a*) Mean velocity profile measurements. (*b*) Mean velocity profiles smoothed with potential core and Gaussian shear-layer distributions. z/d_0: ▼, 0·125; ▲, 0·5; ■, 1·0; ×, 1·5; ●, 2·0.

A survey of the mean jet flow region studied confirmed that it is axisymmetric and approximately parallel throughout the first few diameters in the stream direction.

3. Theory

3.1. *Development of equations*

The initial stages of growth for spatially growing waves in an axisymmetric jet are described using the linearized stability theory. Consider in cylindrical co-ordinates (R, ϕ, Z) a steady axisymmetric jet flow field, having velocity $U(R)$ parallel to the axis of symmetry $R = 0$, and pressure distribution $P(Z)$ in the axial direction. Upon this mean profile we superpose the perturbation velocity and pressure fields.

Non-dimensionalization is achieved using the jet centre-line velocity and the half-breadth thickness of the shear-layer region of the jet velocity profile. The composite motion is, non-dimensionally,

$$\left.\begin{aligned} V_Z(R,\phi,Z,T) &= U(R)+\tilde{V}_Z(R,\phi,Z,T),\\ V_r(R,\phi,Z,T) &= \tilde{V}_r(R,\phi,Z,T),\\ V_\phi(R,\phi,Z,T) &= \tilde{V}_\phi(R,\phi,Z,T),\\ p(R,\phi,Z,T) &= P(Z)+\tilde{P}(R,\phi,Z,T), \end{aligned}\right\} \tag{3.1.1}$$

where tildes denote disturbance quantities that are further decomposed (in the notation of Batchelor & Gill 1962) as

$$\left.\begin{aligned} \tilde{V}_Z(R,\phi,Z,T) &= \mathrm{Re}\{\mathscr{F}(R)\exp[i\alpha Z-i\omega T+in\phi]\},\\ \tilde{V}_R(R,\phi,Z,T) &= \mathrm{Re}\{i\mathscr{G}(R)\exp[i\alpha Z-i\omega T+in\phi]\},\\ \tilde{V}_\phi(R,\phi,Z,T) &= \mathrm{Re}\{\mathscr{H}(R)\exp[i\alpha Z-i\omega T+in\phi]\},\\ \tilde{P}(R,\phi,Z,T) &= \mathrm{Re}\{\mathscr{P}(R)\exp[i\alpha Z-i\omega T+in\phi]\}, \end{aligned}\right\} \tag{3.1.2}$$

where $\alpha = 2\pi/\lambda$ is the wavenumber, λ being the wavelength in the stream direction, ω is the angular frequency, n is the integral mode number and $\mathscr{G}$, $\mathscr{H}$, $\mathscr{F}$ and $\mathscr{P}$ are complex functions of the radial co-ordinate only. According to the spatial theory, α is a complex number, the imaginary part of which indicates growth or decay with the axial co-ordinate. The angular frequency ω is constrained to be only real. Using this constraint, we examine only the spatial growth of the initially infinitesimal disturbances.

The following analysis will be carried out inviscidly, since the instability observed in such two-dimensional mean flows as jets, wakes and shear layers is a dynamic instability. In these flows, viscosity has only a stabilizing effect, as noted from the characteristics of the corresponding neutral curve. Here, a similar assumption is made for the axisymmetric jet.

Substitution of the above quantities into the incompressible continuity and inviscid momentum equations, where mean flow quantities are appropriately extracted, and $\mathscr{H}(R)$, $\mathscr{F}(R)$ and $\mathscr{P}(R)$ are eliminated, gives the governing equation (see Batchelor & Gill)

$$(U-c)\frac{d}{dR}\left[\frac{R}{n^2+\alpha^2R^2}\frac{d(R\mathscr{G})}{dR}\right]-(U-c)\mathscr{G}-R\mathscr{G}\frac{d}{dR}\left(\frac{RU'}{n^2+\alpha^2R^2}\right)=0, \tag{3.1.3}$$

where primes denote differentiation with respect to R, and c is the complex phase velocity where $\omega = \alpha c$. The boundary conditions are

$$\mathscr{G}(+\infty) = \mathscr{G}'(+\infty) = (0, 0), \tag{3.1.4}$$

where the ordered pairs refer to the real and imaginary parts of the complex functions. Kinematically, near the axis of symmetry we find (see Batchelor & Gill)

$$\mathscr{G}(R) \simeq R + \tfrac{1}{12}\alpha^2 R^3 \quad (n = 0), \qquad \mathscr{G}(R) \simeq R^{n-1} \quad (n \neq 0). \quad (3.1.5), (3.1.6)$$

Beyond the edge of the axisymmetric mean profile, the solutions outside the jet have the form

$$\mathscr{G}(R) = CI_1(\alpha R) + DK_1(\alpha R), \tag{3.1.7}$$

where I_1 and K_1 are modified Bessel functions of the first and second kind, respectively. Invoking the infinity boundary conditions, we find in this region

$$\mathscr{G}(R) \simeq K_1(\alpha R) \simeq \frac{\exp\{-\alpha R\}}{(2/\pi\alpha R)^2}, \quad \mathscr{G}'(R) \simeq -[\tfrac{1}{2}R + \alpha]\frac{\exp\{-\alpha R\}}{(2/\pi\alpha R)^2}. \tag{3.1.8}$$

The three eigenvalue problems posed here (viz. for $n = 0$, $n = 1$ and $n = 2$) will be solved numerically in subsequent sections. Our goal is to select the most highly amplified eigenmode. The eigenvalue problems thus formed require but the input of a particular jet mean velocity profile for the determination of the respective dispersion relation. As the mean velocity profile of the jet flow continuously changes in the flow direction, the question arises as to which profile should be used. Since the jet profile changes slowly with downstream direction, we adopt the quasi-uniform assumption.

3.2. *Quasi-uniform assumption*

The velocity measurements presented in figure 3 reveal that the axisymmetric jet velocity profiles to be studied are suitably smoothed by the curves shown. These curves are flat, having a potential core in the centre portion of the jet flow and edges that closely approximate Gaussian functions. With downstream direction, both the potential core region and the Gaussian shear-layer distributions are altered so as to fit the measured profile. The numerical results for these alterations are presented in figure 3.

Given these values for the smoothing curves, the quasi-uniform assumption is now adopted in the near field of the jet flow, where disturbance amplitudes are small. At each stream location where a top-hat, Gaussian-edged profile is selected, the eigenvalue computation is then performed. While this procedure is unreal in the sense that streamwise derivatives of the mean velocity are neglected *a priori*, the collective results for the successive profiles are considered to predict the trends of longitudinal variations in the different mean profiles. Certainly this procedure is an improvement on the usual practice of selecting a single velocity profile somewhere in the flow being examined, computing eigenvalues and sometimes eigenfunctions, then comparing these with measurements made throughout the small disturbance region.

3.3. *Computational procedure*

Adopting the quasi-uniform assumption and choosing a particular mean jet profile, a Runge–Kutta integration with an initially guessed pair (α, ω) was performed between appropriate centre-line conditions and the modified Bessel conditions that exist beyond the jet edge. When the integration results differed from the modified Bessel conditions at the edge of the jet, a Newton–Raphson scheme altered the guess for (α, ω) and the process was repeated until a match occurred. The values for the pair (α, ω) that produced the match were then taken as an eigenvalue pair. This calculation is next done for each of the three centre-line conditions, and for each of five mean profiles beginning near the jet source and extending through five diameters downstream.

The integration procedure was followed using various grid sizes and matching tolerances, until it was found that reducing each of these by a factor of ten changes only the fourth decimal place in α with a fixed ω. The values finally used for grid size and matching tolerance for ordinate and slope at the jet edge were 0·01 and 0·001, respectively.

For the sake of brevity, only the eigenvalue results for a single jet profile will be presented. Here, these results for the characteristics of the various disturbances as well as for the eigenfunctions of velocity and vorticity will be of particular interest, especially for the disturbance which is the most highly amplified at each jet position. According to the linear theory, it is expected that these disturbance characteristics and their eigenfunctions should be observed in the corresponding experimental study.

3.4. *Eigenfunctions*

The solutions to the governing equation are obtained numerically. With specific eigenvalues (viz. those for the most highly amplified disturbances), the eigenfunctions are computed as follows. Taking $\mathscr{F}(R)$ as an example, the actual disturbance has amplitude $|\mathscr{F}|$ and phase $\theta_F(R)$, where

$$\mathscr{F}(R) = |\mathscr{F}(R)| \exp\{i\theta_F\}. \tag{3.4.1}$$

Therefore,

$$\tilde{V}_Z(R, \phi, Z, T) = \mathrm{Re}\{|\mathscr{F}(R)| \exp\{i\theta_F\} \mathscr{F} \exp[in\phi + i\alpha Z - i\omega T]\}. \tag{3.4.2}$$

The distribution of disturbance vorticity will also be determined; the components are, in our notation,

$$\left.\begin{aligned} \gamma_R = i/R[n\mathscr{F}(R) - R\mathscr{H}(R)], \quad \gamma_\phi = -[\mathscr{F}'(R) + \alpha\mathscr{G}(R)], \\ \gamma_Z = \left[\mathscr{H}'(R) + \frac{\mathscr{H}(R)}{R} + n/R\,\mathscr{G}(R)\right], \end{aligned}\right\} \tag{3.4.3}$$

where primes denote differentiation with respect to R.

4. Eigenvalue results

4.1. *Individual jet profiles*

Adopting the quasi-uniform assumption, the individual dispersion relationships are computed throughout the first five diameters of the jet flow for each type of disturbance. A typical result is shown in figure 4 for the jet station $z/d_0 = 0{\cdot}125$.

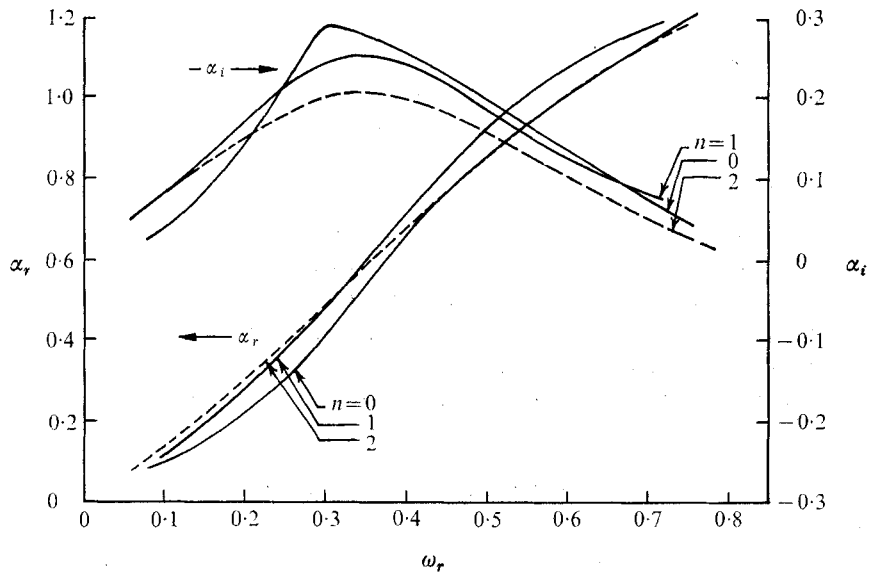

FIGURE 4. Eigenvalue results at $z/d_0 = 0{\cdot}125$.

z/d_0	A	n	$-\alpha_i$	α_r	ω_r	c_p
0·125	4·80	0	0·290	0·411	0·300	0·730
		1	0·250	0·600	0·350	0·583
		2	0·210	0·580	0·340	0·586
2·00	2·80	0	0·255	0·535	0·374	0·699
		1	0·211	0·550	0·350	0·636
		2	0·160	0·564	0·330	0·585
4·00	1·20	0	0·115	0·590	0·450	0·763
		1	0·161	0·567	0·354	0·624
		2	0·063	0·411	0·224	0·545

TABLE 1. Eigenvalue results for the most unstable axisymmetric, helical, and double helical disturbances in an axisymmetric jet

Here, as at all other stations examined, all three types of disturbance are unstable, and all three are dispersive with varying amplification rates. Of these, the most unstable is seen to be the axisymmetric disturbance having characteristics $\alpha_r = 0{\cdot}411$, $\omega_r = 0{\cdot}300$, as a result of its maximum spatial amplification rate, $-\alpha_i = 0{\cdot}290$. The phase velocities for these disturbances, although not presented explicitly, can be found via $c_p = \omega_r/\alpha_r$. It is noted that the phase velocity for the longest axisymmetric disturbances exceeds unity owing to the structure of the shear layer at the edge of the jet. With downstream distance and thicker shear layer, the phase velocity for all disturbances is less than one.

For the sake of brevity, the most unstable disturbance characteristics calculated in the near jet flow are presented in table 1. In the table, it is noted that at jet stations $z/d_0 = 0{\cdot}125$ and $2{\cdot}0$, an $n = 0$ axisymmetric disturbance is the most

unstable of the three types tested. However, at the station $z/d_0 = 4{\cdot}0$, it is found that an $n = 1$ helical disturbance has become the most highly amplified of the three types. Actually, the change-over in the hierarchy of unstable waves occurs at $z/d_0 = 3{\cdot}0$, as a result of the streamwise variations in the spatial amplification rates of the $n = 0$ and $n = 1$ disturbances. The axisymmetric amplification rate decreases more rapidly with stream distance than that of the helical disturbance. As this shear layer thickens to the point where the half-breadth thickness of the shear layer is 55 % of the potential core radius, the helical $n = 1$ disturbance becomes the dominant disturbance in the jet flow.

At no jet station was the $n = 2$ double helical disturbance found to receive maximum amplification. Its maximum amplification rate is seen from the table to occur at the most upstream station; and from this maximum there is observed to be a rather rapid decrease throughout the near jet flow field.

4.2. *Eigenfunction computations*

Having the characteristics of the most highly amplified disturbances at successive jet stations, we now examine the cross-stream distributions of the corresponding eigenfunctions. These distributions will exclude the travelling wave portion of the disturbance and the spatial amplification factor; the distributions will include the exponential factor $\exp\{in\phi\}$, representing azimuthal phase variations. The three components of velocity and vorticity will be presented for the axisymmetric disturbance mode at the most upstream jet station only. The components for the helical mode are presented only for the station $z/d_0 = 4{\cdot}0$.

In the plots presented below, the ordinates are scaled with respect to the conditions imposed upon the ordinate or slope of the function $\mathscr{G}(R)$ at the jet centre-line. As such, each of the eigenfunction distributions has to be appropriately scaled according to the ratio of the corresponding experimental values.

For the $n = 0$ axisymmetric disturbance mode, the disturbance velocity and vorticity components at jet station $z/d_0 = 0{\cdot}125$ are shown in figure 5. The azimuthal component of the disturbance velocity, together with radial and streamwise components of disturbance vorticity, are zero across the diameter of the jet. From the graph of the streamwise component of disturbance velocity, there exists a phase shift near the edge of the jet. It is also noted that both the streamwise and radial components of disturbance velocity have a small peak just inside the absolute maximum in the distribution. These small peaks are the result of the sharp change in the curvature in the mean profile at the outer edge of the potential core [see (2.2.1)]. This is also noted in the azimuthal component of disturbance vorticity, which exhibits large, initially negative peaks at these locations. Of course, with time, these distributions will oscillate with angular frequency; and with downstream disturbance they will have a wavelength in accordance with the travelling wave portion of the disturbance that is omitted from these graphs.

Downstream at $z/d_0 = 4{\cdot}0$, where the helical mode is the most amplified, the cross-stream distributions of disturbance velocity and vorticity are presented in figure 6. Here, the non-dimensional radial co-ordinate is shown reduced,

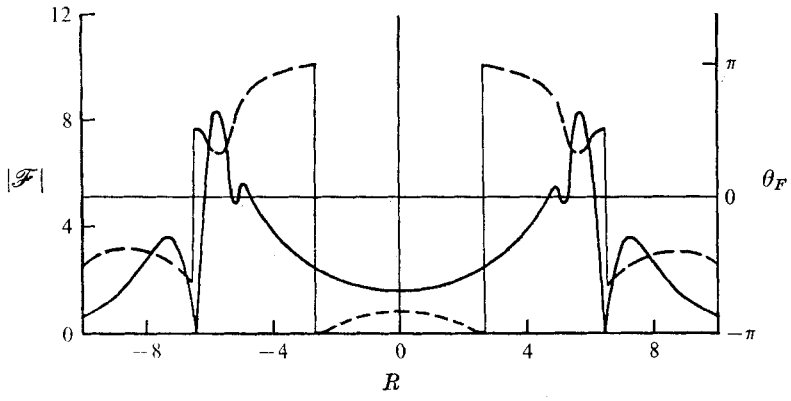

(*a*)

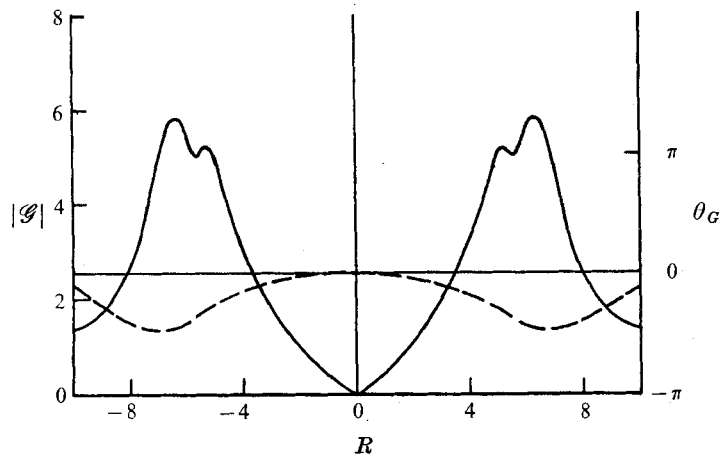

(*b*)

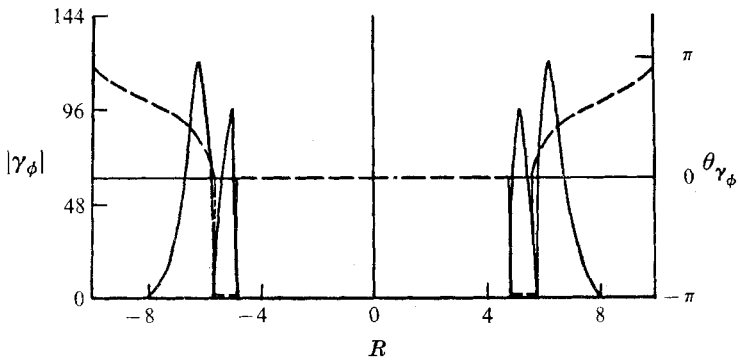

(*c*)

FIGURE 5. Eigenfunction distributions for $n = 0$ at $z/d_0 = 0{\cdot}125$.

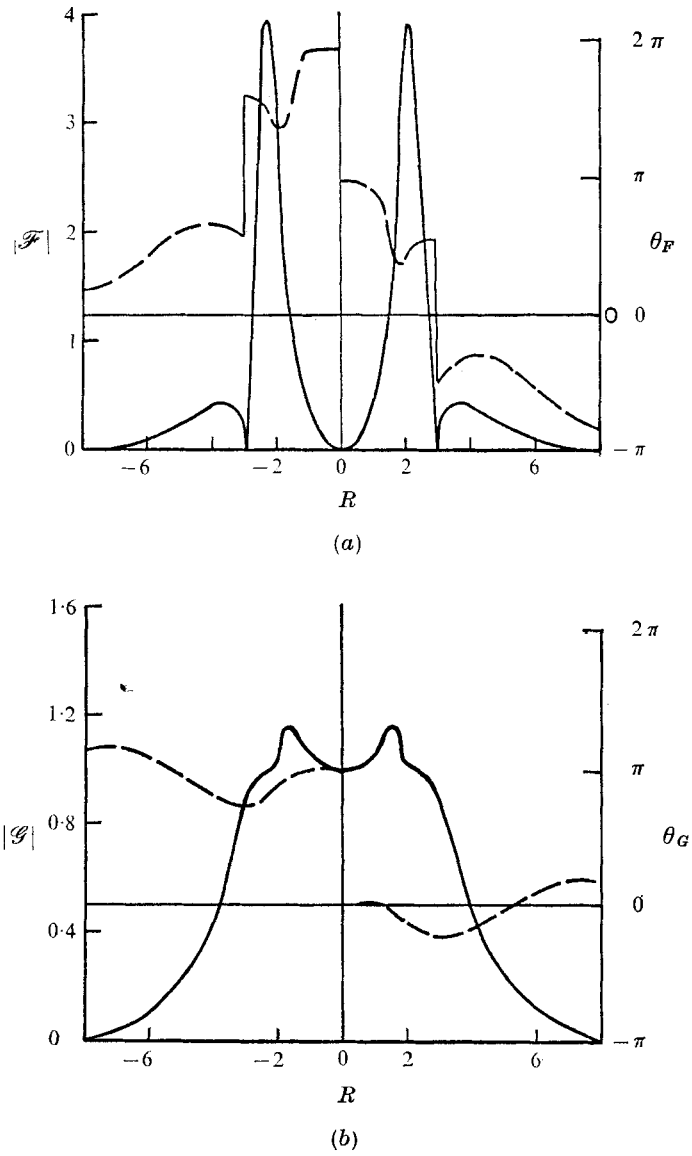

FIGURES 6(a, b). For legend see page 554.

compared with figure 5, by virtue of the choice of characteristic length. Examining the radial and streamwise components of disturbance velocity, they are found to have amplitudes that are qualitatively quite similar to the corresponding distributions for the axisymmetric mode at station $z/d_0 = 0{\cdot}125$. However, through the exponential factor containing the azimuthal angle, there exists a phase shift of π radians at the centre-line for all the helical eigenfunctions. Comparing qualitatively the radial components of disturbance velocity in the axisymmetric mode with the helical, it is noted that again small peaks occur in $\tilde{V}_R$ or $i\mathscr{G}$ at the radial positions where the mean profile has large negative curva-

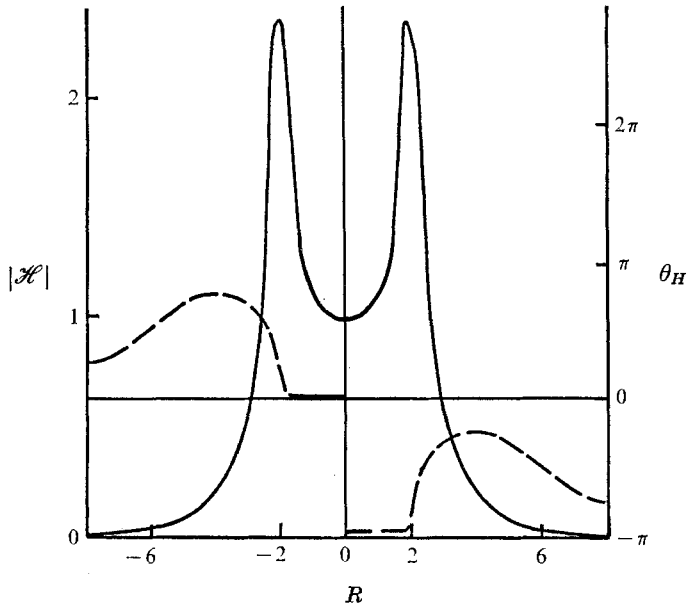

(c)

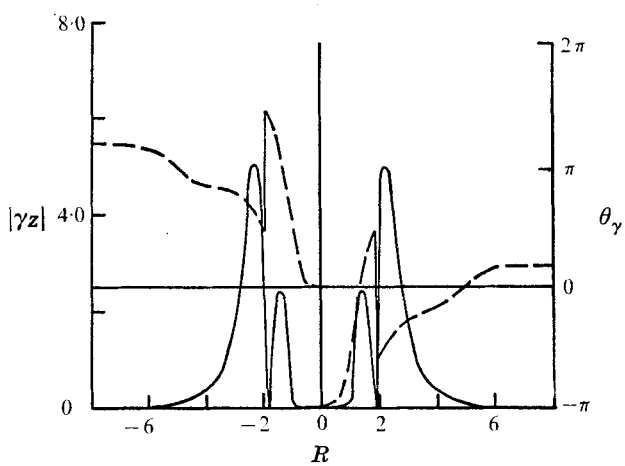

(d)

FIGURES 6(c, d). For legend see page 554.

ture. The streamwise distributions for the two modes indicate that the minor peaks disappear completely at the downstream station. At $z/d_0 = 4{\cdot}0$, in the azimuthal component of disturbance velocity, it is found that there exists only a single peak on each side of the centre-line, with a single π radian shift on the centre-line. The azimuthal component of disturbance vorticity for the helical mode is also found to be qualitatively similar to that for the symmetrical mode, excluding the phase shift at the centre-line. For the helical mode, there is found a quantitative reduction in these peaks which are located at the radial position

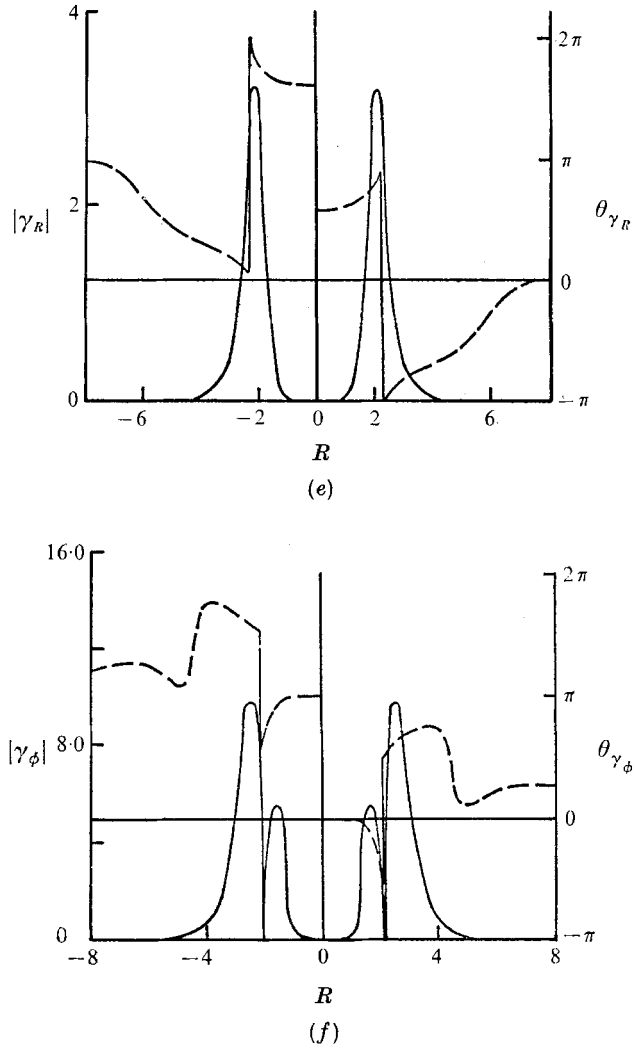

FIGURE 6. Eigenfunction distributions for $n = 1$ at $z/d_0 = 4{\cdot}0$.

of the maximum shear layer in the mean velocity profile. However, it is recalled that the exponential amplification factor has been excluded from these results. This factor comprises a gain of about 890 over the first four diameters of jet flow, which more than compensates for the apparent decrease between figures 5 (*c*) and 6 (*f*), and indicates the nature of the spatial amplification.

5. Measurement of disturbance characteristics

Measurements of disturbance characteristics (viz. wavelength, frequency, and the cross-stream r.m.s. distributions of the streamwise component of the disturbance velocity) were made using anemometry. In addition, surveys were conducted to determine the azimuthal and radial phase relationships of $\tilde{V}_Z$. Values of

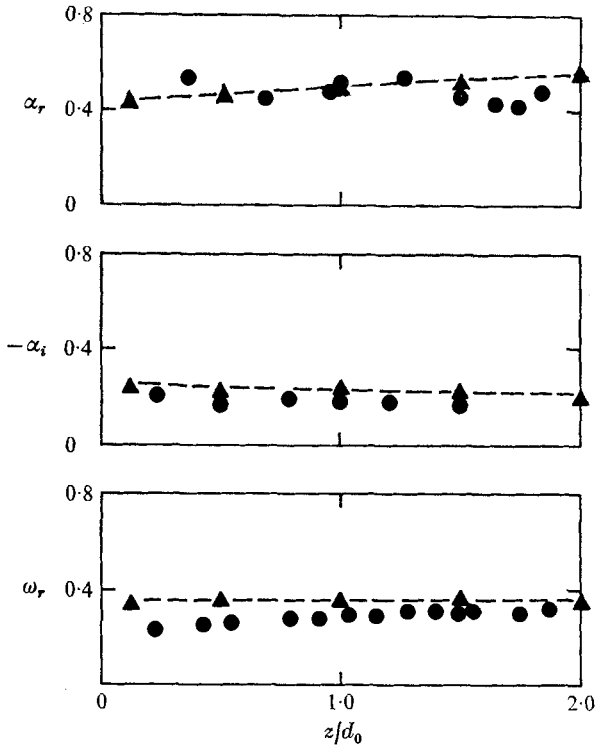

FIGURE 7. Comparison of experimental values (●) of disturbance wavenumber, amplification rate and angular frequency with the results of the spatial theory (▲).

the spatial growth rate $-\alpha_i$ were calculated from the r.m.s. distributions, using the finite difference ratio

$$-\alpha_i = \Delta \log_e [(\overline{\tilde{V}_Z^2})^{\frac{1}{2}}/U_{\mathbb{C}}] (\Delta Z)^{-1}, \tag{5.1}$$

where the bar indicates the time average.

In figure 7, experimentally determined values for disturbance wavenumbers are presented for the most highly amplified disturbances, according to the previously described theory. The experimental values were determined by traversing one sensor longitudinally relative to another one, until a phase shift was visually observed on a dual-trace oscilloscope. Actually, by inverting one signal, one only needs to traverse half a wavelength in the stream direction to obtain the required shift. The resulting streamwise separation of the sensors is then recorded as half the wavelength for the station halfway between the two sensors. As indicated in table 1, over the first few diameters of the jet flow, the most highly amplified wavenumber, according to the theory, increases with downstream distance. Thus the disturbance wavelength decreases over this streamwise distance. The scatter found in the experimental results presented in figure 7 is attributed, for the most part, to natural variations or drift of the disturbance characteristics. This drifting is especially acute in the very near jet region, where disturbance amplitudes are very small.

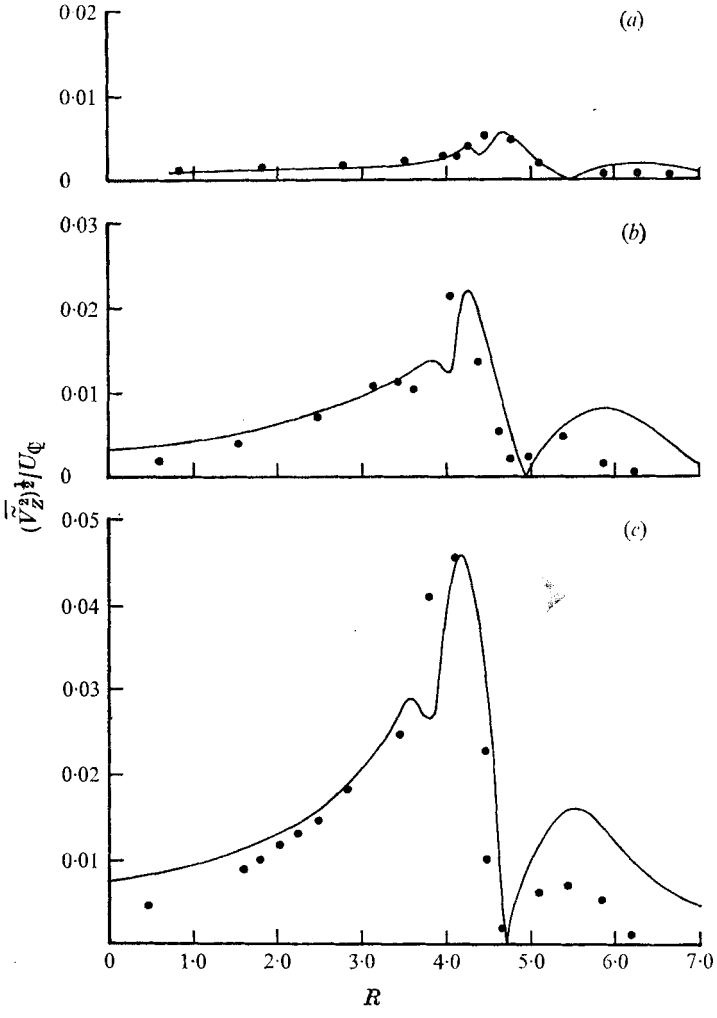

FIGURE 8. Cross-stream distribution of $(\overline{\tilde{V}_Z^2})^{\frac{1}{2}}/U_{\mathbb{C}}$. z/d_0: (a) 1·0, (b) 1·5, (c) 2·0.

Figure 7 also presents the values for spatial growth rate as calculated from the cross-stream r.m.s. distributions of $\tilde{V}_Z$. The quantitative agreement of the theoretical and experimental results is considered good. Cross-stream distributions of $\tilde{V}_Z$ are presented in figure 8 for several jet stations, where the solid lines are the theoretical eigenfunctions scaled for the purposes of qualitative comparison to match the experimental results at the maximum value. Of course, quantitatively, a multiplicative constant for the eigenfunctions is omitted from the above theory; hence the eigenfunction distributions are simply scalar multiples of the results shown in figure 8. The qualitative nature of these cross-stream distributions does not conclusively indicate which type of disturbance is amplifying naturally in the near jet field. This is described below in the measurements of disturbance phase.

Using a single channel of anemometry, a survey of disturbance angular

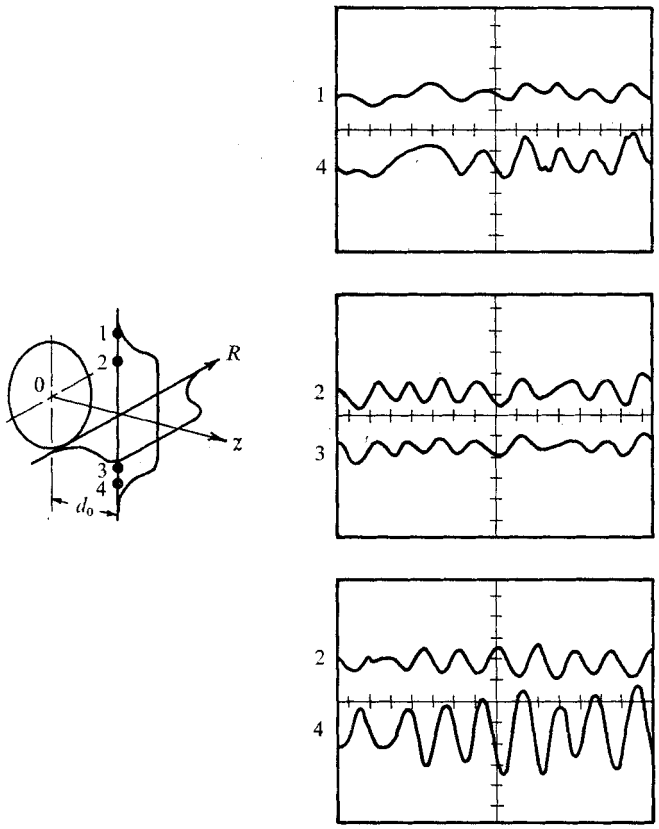

FIGURE 9. Diametral distribution of the streamwise component of disturbance velocity at $z/d_0 = 1{\cdot}0$.

frequency in the near jet region produced the experimental values shown in figure 7, where the theoretical values of the most highly amplified disturbances are also presented. The theoretical values, as listed in table 1, indicate that angular frequency increases slightly with downstream distance over the first two diameters of the jet flow. This trend is in agreement with the experimental values, which show improved agreement with downstream distance. It is noted that with the exception of the wavenumber value at $z/d_0 = 0{\cdot}3$, all of the experimentally determined disturbance characteristics fall below the corresponding theoretical values. This is as expected, for the theory is an inviscid one while the experiment is conducted at finite Reynolds number.

With an additional channel of anemometry, an investigation of the disturbance phase was conducted one diameter from the jet source. In figure 9 are presented tracings of oscillographic records which exhibit typical anemometer signals from probes placed along a diameter of the jet flow. From these and other similar records it is concluded that there does exist a phase shift of π radians in the shear-layer region of the jet flow. Further, from the two upper tracings there exists phase agreement in the outer region of the jet as well as in the central portion, just beyond the potential core. Figure 10 presents similar oscillographic tracings

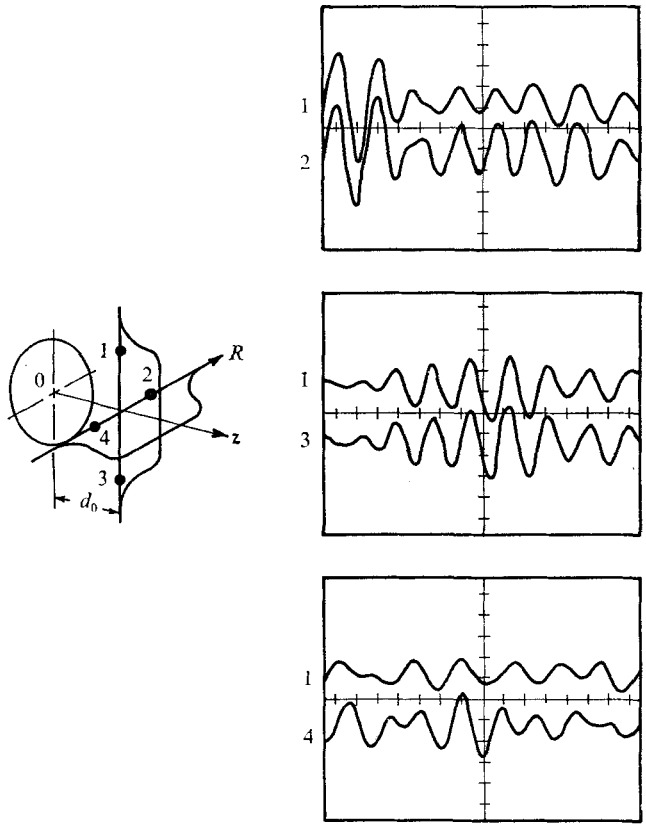

FIGURE 10. Azimuthal distribution of the streamwise component of disturbance velocity at $z/d_0 = 1{\cdot}0$.

recorded from sensors placed entirely within the radial location of the phase shift established through the results in figure 9. It is seen from these results that the disturbance phase in the shear layer beyond the potential core radius, and within the location of the phase shift, exhibits complete agreement. This confirms the existence of an axisymmetric disturbance in the near jet field. An additional observation that can be made from figures 9 and 10 is the intermittency or natural drift in both frequency, amplitude, and sometimes in phase that is visible in these oscillographic records.

An attempt was made to determine the disturbance phase distribution at jet station $z/d_0 = 4{\cdot}0$. However, no firm conclusions can be drawn from these results. Suffice it to report that approximately half the records indicate that the axisymmetric mode prevails and the other half point to the helical mode. Although there does exist the above-mentioned natural drift, there was observed no trend toward a double helical disturbance. Perhaps this apparent confusion as to the natural selection of a dominant mode is the result of the quantitatively similar amplification rates of the axisymmetric and helical modes at this location in the jet (see figures 4, 7; table 1).

6. Discussion and conclusion

The theoretical results of the present work are considered to be in good agreement with the corresponding experimental observations. One of the most important conclusions to be drawn from our effort is that the detailed structure of the mean velocity profile is quite critical to the results of the spatial stability analysis. Therefore, it is concluded that the large values for phase velocity predicted by Crow & Champagne are the result of their choice of a 'top-hat' profile, with its infinitely thin shear-layer region at the edge of the jet. Furthermore, in the present effort several interesting results are obtained by incorporating into the theory (through the quasi-uniform assumption) the streamwise variations in the jet's potential core and shear-layer thickness.

It is found that initially in the jet there exists an axisymmetric disturbance which dominates the other two modes considered, namely the helical and double helical modes. With downstream distance, this dominant disturbance exhibits a slightly increasing wavenumber and angular frequency. It is amplified with a spatial rate that is found to diminish slightly in the stream direction. Each of these trends agrees quantitatively and qualitatively with the experimental results.

Further, with downstream distance at the three-diameter station, it is found that according to the linear spatial stability theory, the helical mode of instability becomes the most highly amplified. This is due to the different streamwise variations of the spatial growth rates of these two disturbances. Throughout the following two diameters of the jet flow, the helical mode remains the most dominant. This switch in the hierarchy of unstable disturbances could not be conclusively documented experimentally, owing to either the usual natural drift or the intermittency in the alternation from one mode to the other. The axisymmetric and helical modes of disturbance are found to have quantitatively very similar disturbance characteristics, such as wavenumber, frequency and spatial amplification rates in this portion of the jet flow. The other mode of disturbance considered in the present study, the double helical mode, was found to be unstable through the jet region examined, but at no jet location was it found to dominate.

Because of the change of the most unstable disturbance mode in the axisymmetric jet, and because, initially, the unstable disturbances of interest in the jet are infinitesimal, the use of artificial excitation of a single 'naturally amplifying' mode is considered less than desirable. Such excitation has been resorted to in the past, to lock the drifting disturbance characteristics onto their natural values. In the present results, although this drift is apparent, it is felt that to employ patiently lengthy averaging times is the more appropriate of the two responses.

To interpret properly this switch in the hierarchy of unstable modes, one has to make the assumption that the linear theory applies throughout the first three diameters of jet flow. Then, through the principle of superposition, the previously dominant and exponentially amplifying axisymmetric disturbances are dominated by a previously less dominant helical mode. In all the preceding jet flow it is inherently assumed that, although exponentially amplifying, no disturbance

has grown sufficiently either to interact with any other or to nullify the linear assumption. As such, no mechanisms or details of the mode switch are given.

However, it seems appropriate to conclude that, with downstream distance, the developments that occur both in the present axisymmetric jet, and quite probably in other unstable flows, result from phenomena that initiate in regions where disturbances are small. As such, it is appropriate to understand all the characteristics of the unstable disturbances throughout the linear region before attempting the nonlinear theory or the numerical computation of these exceedingly complex flows.

The authors gratefully acknowledge the support of the National Science Foundation through contract GK 1288, which assisted in funding this work.

REFERENCES

BATCHELOR, G. & GILL, A. 1962 Analysis of the stability of axisymmetric jets. *J. Fluid Mech.* **14**, 529.

CROW, S. & CHAMPAGNE, F. 1971 Orderly structure in jet turbulence. *J. Fluid Mech.* **48**, 547.

FREYMUTH, P. 1966 On transition in a separated laminar boundary layer. *J. Fluid Mech.* **25**, 683.

GASTER, M. 1968 Growth of disturbances in both space and time. *Phys. Fluids*, **11**, 723.

GILL, A. 1962 On the occurrence of condensations in steady axisymmetric jets. *J. Fluid Mech.* **14**, 567.

MATTINGLY, G. E. 1966 The hydrogen bubble visualization technique. *Dept. of Navy, David Taylor Model Basin, Rep.* no. 2146.

MATTINGLY, G. E. 1968 The stability of a two-dimensional incompressible wake. *Dept. of Aerospace and Mechanical Sci., Princeton University, Rep.* no. 858.

MATTINGLY, G. E. & CRIMINALE, W. 1972 The stability of an incompressible two-dimensional wake. *J. Fluid Mech.* **51**, 233.

REYNOLDS, A. J. 1962 Observations of a liquid-into-liquid jet. *J. Fluid Mech.* **14**, 552.

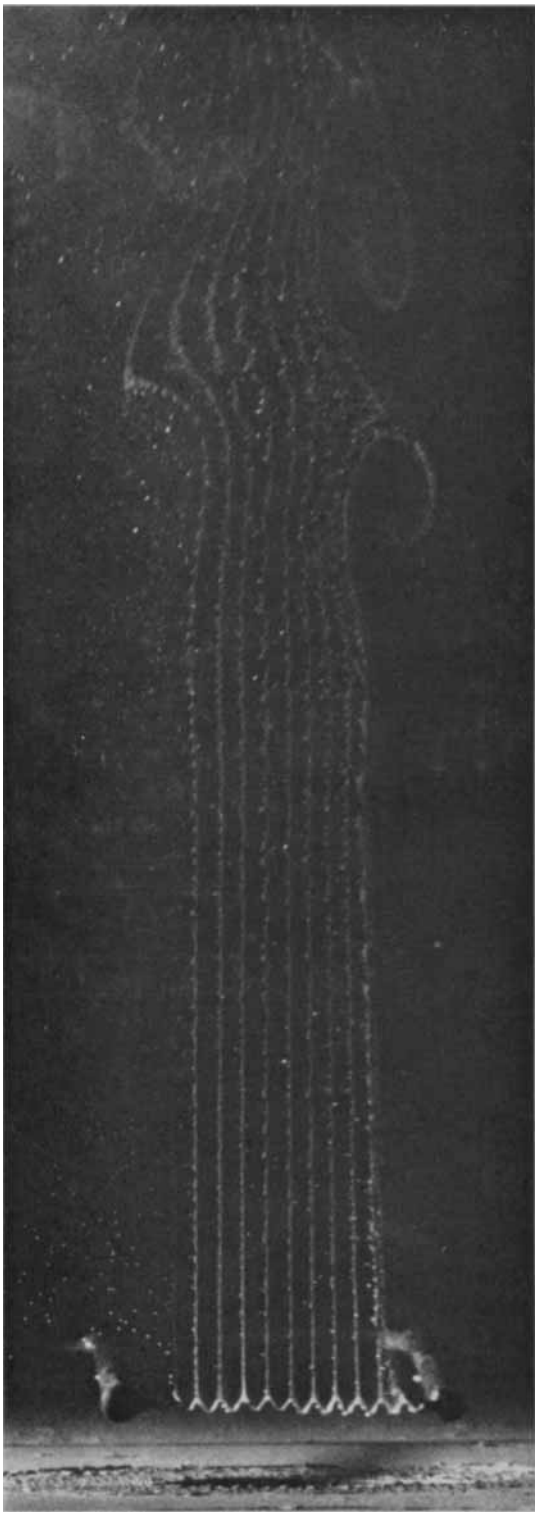

FIGURE 1. Jet flow visualized with hydrogen-bubble technique. Flow is from left to right with kinked bubble-generating wire just downstream of jet source.